

1563 An Accurate Method for Determination of Tissue Thickness in Paraffin Blocks by Faxitron Analysis: Application to Tissue Microarray Construction
Y Zhao, X Kong, M Ksionsk, PD Walden, MC Bosland, J Melamed. NYU School of Medicine, New York, NY.

Background: The determination of tissue thickness in paraffin blocks in the histology laboratory has been largely based on visual estimates. More accurate methods are required for triage of paraffin embedded tissue for special studies and research applications. This is particularly crucial for tissue microarray (TMA) construction, where thin tissue from donor blocks can result in short TMA cores that are likely to disappear after few sections. Using an accurate method for thickness determination, one could include additional cores or avoid inadequate donor block material. We have developed an accurate method to determine thickness in donor paraffin blocks used for prostate cancer TMA construction as part of the NCI Cooperative Prostate Cancer Tissue Resource.

Design: Paraffin blocks of radical prostatectomy specimens (n = 247) assembled from 4 collaborating institutions were used for construction of 4 prostate cancer TMAs. All donor blocks were x-rayed after TMA construction using a digital Faxitron instrument, with vertical block alignment on the detector window. Digital radiograph images were manipulated to enhance contrast and to obtain linear measurements of the tissue at the TMA needle sites. The TMA blocks were cut into consecutive numbered 4 micron-thick sections through the entire block. The thickness of the individual cores determined radiographically was correlated with presence or loss of cores in the 150th TMA slide (from the final third of the TMA block).

Results: In the 150th slide derived from the 4 TMA blocks, 202 of 1388 cores (14.5%) were no longer present. The mean thickness of the paraffin embedded donor tissue corresponding to the absent cores was 1.54 mm as compared to 2.12 mm for the donor tissue corresponding to the preserved cores (p < 0.01). With increasing sections through a block, there was an increase in the number of lost cores with an inverse correlation between thickness of the donor block and loss of cores.

Conclusions: Accurate determination of tissue thickness in paraffin blocks can be obtained using Faxitron equipment which is available in many pathology laboratories. This type of determination is a valuable aid in construction of TMAs for large scale use. Prior knowledge of tissue thickness in TMA construction can prompt compensatory steps to enhance the yield of valuable samples and assure sufficient numbers of retained cores for statistical analysis in biomarker evaluations.

1564 Non-Invasive Prenatal RHD Genotyping by Real-Time PCR Using Plasma from RHD-Negative Pregnant Women

L Zhou, J Thorson, CE Nugent, RD Davenport, WJ Judd. University of Michigan, Ann Arbor, MI.

Background: Prenatal determination of fetal *RHD* genotype has become an important aid to the management of hemolytic disease of the newborn (HDN) due to maternal anti-D antibodies. Invasive procedures to obtain fetal genetic material for prenatal testing carry significant risks; therefore, non-invasive alternatives for the prenatal determination of fetal *RHD* genotype have been actively pursued. In this study we used a real time PCR-based assay to determine the fetal *RHD* genotype from cell free fetal DNA in maternal plasma.

Design: Peripheral blood samples were collected from 98 Rh-negative pregnant women. Cell-free DNA was extracted from the plasma and assayed for the presence of exons 4, 5, and 10 of the *RHD* gene by real-time PCR. The presence of fetal DNA in the samples was confirmed by the detection of the *SRY* gene on the Y chromosome in cases with a male fetus. If the PCR results for both the *RHD* and *SRY* genes were negative, the presence of fetal DNA was confirmed by demonstrating distinctions between cell free plasma DNA and maternal buffy coat DNA in their genotypes of 10 biallelic insertion/deletion polymorphisms. *RHD* genotyping results were compared with results from serological determination of the newborn's RhD phenotype.

Results: Seventy-two Rh-positive babies and 26 Rh-negative babies were identified by serological studies. *RHD* was detected in the maternal plasma of D-positive fetuses using exon 4, 5 and 10 primers in 69/72, 71/72, and 72/72 samples, respectively. None of the maternal plasma samples from the 26 Rh-negative fetuses were positive for *RHD* by the real time PCR assay. The presence of fetal DNA in the maternal plasma of D-negative fetuses was confirmed by the detection of *SRY* (10/10 boys). Distinctive genotypes for insertion deletion polymorphisms confirmed the presence of fetal DNA in 14 of 16 cases of female fetuses.

Conclusions: Using real-time PCR assays for the *RHD* gene in combination with assays for the *SRY* gene and a group of biallelic insertion/deletion polymorphisms, we obtained an accuracy of 94% in predicting fetal Rh D status in our study. Discrepancies between serology and PCR were attributable to the absence of amplifiable fetal DNA in a small number of maternal plasma samples. This assay provides a rapid and accurate assessment of fetal *RHD* genotype while avoiding the significant risks of invasive sampling procedures.

Ultrastructural

1565 Globular Hepatic Amyloid

N Agram, J Shia, D Klimstra, N Lau, R Erlandson, O Lin, D Filippa, T Godwin. Memorial Sloan-Kettering Cancer Center, New York; Washington Hospital Center, Washington, DC.

Background: Hepatic amyloid deposition in the form of globular inclusions is a rare occurrence. Its clinical and pathological significance is undefined, and its histologic appearance can cause diagnostic confusion.

Design: The clinical and pathological findings of a case of globular hepatic amyloid in a patient with B cell lymphoma and chronic hepatitis C are described, and relevant literature data is reviewed.

Results: The patient was a 64-year-old male, found to have abnormal liver function tests and positive HCV serology during a blood workup for his known B cell lymphoma. The lymphoma was diagnosed five years earlier and was in remission after chemoradiation. A liver biopsy to assess HCV disease revealed minimally active chronic hepatitis with mild periportal fibrosis. The liver also contained unusual intracytoplasmic globular inclusions within hepatocytes and stromal cells. These pale eosinophilic globules ranged from a few micrometers to 40 micrometers in diameter, and were homogeneous or laminated. Congo red stain and ultrastructural studies indicated that these globules were composed of amyloid. Linear form amyloid around vessels was also detected on Congo red stain and on EM. A subsequent fat pad fine needle aspiration demonstrated amyloid around vessels in the abdominal fat. Twenty-four reported globular hepatic amyloid cases have been described in association with a variety of medical conditions. Extra-hepatic organ involvement was not demonstrated in any of the reported cases except in one autopsy series. None of the reported cases were related to immunoglobulin light chain disease, nor did any patient present initially with clinical symptoms that would raise concern of amyloidosis.

Conclusions: Globular hepatic amyloid has a distinct morphologic pattern. Recognition of such a pattern is important in applying appropriate diagnostic modalities such as Congo red stain and electron microscopy. While the histogenesis of globular amyloid deposits remains undetermined, in some cases it may represent an early stage or mild form of systemic amyloidosis.

1566 Renal Tumors in Hereditary Leiomyomatosis Renal Cell Carcinoma Syndrome: Ultrastructural Characterization

A Ahmed, C Torres-Cabala, M Linehan, M Merino, M Tsokos. National Cancer Institute, Bethesda, MD; Center for Cancer Research, Bethesda, MD.

Background: Hereditary Leiomyomatosis Renal Cell Carcinoma (HLRCC) syndrome is a recently described familial syndrome characterized by germline mutations in the *fumarate hydratase* gene predisposing to multiple cutaneous and uterine leiomyomas and renal cell carcinoma. Renal cell carcinomas in patients with HLRCC have a distinct histology and aggressive clinical behavior. Their ultrastructural features have not been previously described.

Design: Tissue from three renal tumors from three patients with confirmed HLRCC syndrome was studied. Representative areas from all three tumors were fixed in buffered glutaraldehyde and processed for ultrastructural analysis.

Results: All three patients were males 40 (two patients) and 64 years of age and had undergone nephrectomy procedures. Two of them were members of the same family. Metastatic disease in the surrounding muscles and omentum was present in two cases. The tumors had a spectrum of morphologic changes including papillary type II morphology with cystic and solid areas. The characteristic nuclear appearance was present in all three cases. All tumors exhibited common ultrastructural features. Specifically, they were composed of clusters of cuboidal cells forming tubular structures and surrounded by multilayered basal lamina. The tumor cells exhibited short apical villi and basal infoldings. The intercellular spaces were widened. The cytoplasm contained numerous mitochondria and abundant often dilated endoplasmic reticulum. Lipid droplets were variable but usually seen in low amounts. Glycogen and lysosomes were present as well. The nuclei were irregular and often exhibited prominent nucleoli. One tumor exhibited in addition some intracytoplasmic vesicles and sparse clusters of intermediate filaments indicative of tonofilaments. Inter-epithelial junctions were common.

Conclusions: Renal tumors in HLRCC patients have unique ultrastructural features suggestive of origin from distal segments of the nephron. They also have a high mitochondrial content, possibly due to their genetic abnormality in an enzyme involved in the Krebs cycle.

1567 Adult Benign Cystic Renal Lesions-Electron Microscopic Studies with Histogenetic Correlations

T Antic, R Fresco, MM Picken. Loyola University Medical Center, Maywood, IL.

Background: Adult cystic nephroma (ACN) is a rare tumor composed of cysts separated by thin septa containing loose stroma with fibroblasts and, focally, cells resembling smooth muscle. The epithelial lining in ACN is hobnail or attenuated and an origin in the distal nephron has been postulated. Mixed epithelial and stromal tumor of the kidney (MESTK) is a recently recognized rare tumor composed of intimately admixed tubules and spindle cell stroma that resembles ovarian. The tumor is usually benign and no blastema, mitoses or atypia are seen. The tumor origin is debated and recently an origin in the distal nephron has been postulated.

Design: We performed detailed morphologic studies, including routine histology, immunohistochemistry and electron microscopy (EM) in four benign adult cystic lesions. Three tumors were classified as MESTK and one as ACN. All tumors were from females.

Results: By routine histology the spindle cell stroma was dense and abundant in MESTK while in ACN only focal microscopic foci were seen. By immunohistochemistry, spindle cell stroma was diffusely positive for smooth muscle actin (SMA) in MESTK and only focally in ACN. By EM, smooth muscle differentiation was seen. Stain for inhibin was negative in all four lesions. In MESTK (3 lesions) the epithelial lining was heterogeneous with focal features compatible with the proximal nephron while other tubules showed features of the loop of Henle (thin segment) or even the collecting duct. In contrast, epithelium in ACN showed only features of the distal tubule and the loop of Henle. By immunohistochemistry, in MESTK focal positivity for CD10, ck7 and high molecular weight keratin was seen. In contrast, in ACN, only positivity to ck7 was present.

Conclusions: Although the stroma in both lesions morphologically resembles ovarian, it does not show the corresponding immunophenotype. By immunohistochemistry and EM, spindle cell stroma shows smooth muscle differentiation in both lesions. However, there are differences in the amount of stroma between the 2 lesions. By EM and immunohistochemistry, the epithelial lining in MESTK has a varied ultrastructure and immunophenotype corresponding to different segments of the nephron. This suggests that the epithelial component in MESTK may be entrapped rather than a part of the tumor itself. In contrast, the epithelial lining in ACN is immunophenotypically and morphologically more consistent with distal nephron derivation. Further studies are needed to elucidate the relationship and criteria for the differential diagnosis between these two lesions.

1568 Lipofuscin Content as a Marker Differentiating Renal Oncocytoma from Renal Cell Carcinoma, and for Estimating Metastatic Potential of Carcinoids

H Chen, ND Cassai, B West, GS Sidhu. New York University School of Medicine, New York, NY; New York Harbor Healthcare System, New York, NY.

Background: "Lipofuscin represent(s) residual bodies left behind in the cell after lysosomal activity. . . It is my experience that cells of most malignant tumors lack lipofuscin granules; only rarely is a small lipofuscin granule seen." (Ghadially, 1997). Slowly growing cells accumulate lipofuscin (LF); faster growing cells have less. Malignant cells have faster turnover rate than benign ones. We test the hypothesis that metastatic carcinoids and renal cell carcinomas will have less LF compared to non-metastatic carcinoids and oncocytomas, respectively.

Design: Five carcinoids, 7 metastatic carcinoids, 4 renal oncocytomas, and 4 renal cell carcinomas, granular cell type were examined ultrastructurally. LF amount was scored as 0 to 3+, with 0 indicating no LF, and 3+ indicating the highest amount.

Results: LF scores were: Oncocytomas (2-3+), renal cell carcinomas (0-1+), non-metastatic carcinoids (1-3+), metastatic carcinoids in local lymph nodes (0-2+), and in distant sites - 2 liver and 1 neck - zero.

Conclusions: LF is decreased in metastatic carcinoids (markedly in distant as compared to local metastases) and renal cell carcinoma as compared with nonmetastatic carcinoids and oncocytomas, respectively. Prediction of metastatic potential in carcinoids and diagnosis of renal cell carcinoma of the granular cell type are a challenge to pathologists. No biological or immunohistological markers exist for differentiating renal oncocytoma from renal cell carcinoma of the granular cell type, or for predicting metastatic potential of carcinoids. This study demonstrates that LF quantitation by electron microscopy can be pivotal in differentiating oncocytoma from renal cell carcinoma, but is of only moderate value for predicting metastatic potential of carcinoids.

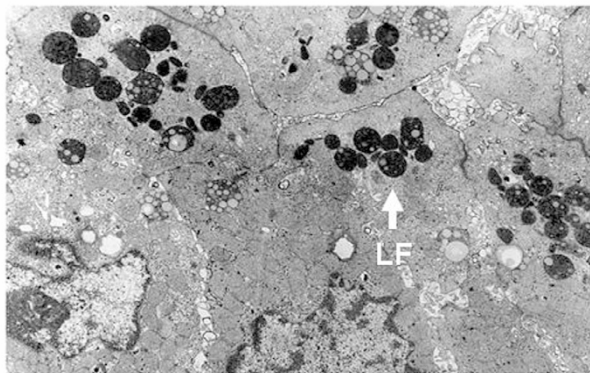


Fig 1. Renal Oncocytoma

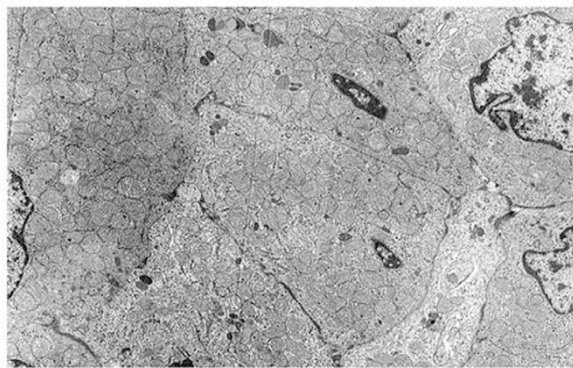


Fig 2. Renal Cell Carcinoma, Granular Cell Type

1569 Sclerosing Rhabdomyosarcoma in Pediatrics: A Matrix-Rich Rhabdomyosarcoma Variant

J Hicks, E Popek, A Heerema, D Lopez-Terrada. Texas Children's Hospital, Baylor College of Medicine, Houston, TX.

Background: Sclerosing rhabdomyosarcoma is a recently described matrix-rich rhabdomyosarcoma variant with a prominent pseudovascular pattern that may be mistaken for osteosarcoma, chondrosarcoma, angiosarcoma, sclerosing synovial sarcoma or undifferentiated sarcoma (Virchows Arch 2000;436:305; Am J Surg Pathol 2002;26:1175; Pediatr Dev Pathol 2004;7:391). Reportedly, a high proportion of tumor cells express MyoD1, with a small proportion reacting with myogenin and desmin. Currently, 7 adult patients with a mean age of 38 years and a single 3 year-old child have been reported with this unique neoplasm.

Design: Review of all rhabdomyosarcoma cases from the surgical pathology and consult files over the past 25 years at Texas Children's Hospital yielded 6 cases (3M:3F, age range 7-16 yrs) which had features of the sclerosing rhabdomyosarcoma variant. Most patients were adolescent (13-16 years) with one patient being 7 years of age. Sites involved included pelvis (2), thigh (2), and head/neck (2). Pulmonary metastases were present at time of diagnosis with 3 patients. Tissue was available for immunocytochemistry and electron microscopy.

Results: Tumor cells were embedded in a hyalinized (1/6) to chondroid-like (2/6) to osteoid-like (3/6) matrix. A pseudoalveolar architectural pattern was noted with 3 tumors. All tumors showed focal desmin, focal muscle specific actin and focal to moderate myogenin immunoreactivity. MyoD1 and smooth muscle actin were moderately positive with 4 tumors and moderately to focally positive in 2 tumors. With all tumors, electron microscopy revealed infrequent tumor cells with actin myofilaments, dense bodies, thick and thin myofilaments and rare z-band material. Many of the tumor cells were round to ovoid and lacked tumor defining ultrastructural characteristics. Cytogenetics was performed in 4 cases and all had complex karyotypes (chromosomal gains and losses with 48 to 158 chromosomes). Alveolar rhabdomyosarcoma translocations (PAX3-FOXA, t[2;13]) were identified in 2 cases. **Conclusions:** Although sclerosing rhabdomyosarcoma may mimic other sarcomas and express myogenic markers only to a limited degree, ultrastructural examination of the tumors provides definitive evidence for skeletal muscle progenitor cell origin. A certain proportion of sclerosing rhabdomyosarcomas possess one of the PAX-FOXA translocations characteristic for alveolar rhabdomyosarcoma, and may represent particularly aggressive tumors.

1570 Ribonucleotide Reductase p53R2 Deficiency and Rapid Onset Renal Failure: Murine Model with Ultrastructural Correlation

J Hicks, P Vogel, D Powell. Texas Children's Hospital, Baylor College of Medicine, Houston, TX; Lexicon Genetics Incorporated, Woodlands, TX.

Background: *Rrm2b* gene encodes ribonucleotide reductase p53R2 that catalyzes the rate-limiting step in deoxyribonucleotide generation required for DNA synthesis and repair. p53R2 is induced by wild type p53 in response to DNA damage. A murine model with *Rrm2b* gene deficiency develops severe proteinuria, hypoalbuminemia and renal failure with death by 14 weeks of age.

Design: *Rrm2b* deficient mice (homogygotes *Rrm2b*^{-/-}) were generated on a mixed murine lineage (129/SV-C57BL/6J). Kidneys were harvested from 10 *Rrm2b* deficient (*Rrm2b*^{-/-}) and 5 wild-type *Rrm2b* competent (*Rrm2b*^{+/+} control) animals at 8 weeks of age. The kidney tissue was harvested for routine light microscopy (formalin-fixation) and electron microscopic (glutaraldehyde fixation) examination. Serologic analyses were also performed (creatinine, BUN, albumin, cholesterol, triglycerides).

Results: Serologic studies were suggestive of renal failure and nephrotic syndrome in *Rrm2b* deficient animals (Cr 1.0, BUN 97.8, albumin 1.5, cholesterol 627, triglycerides 478) compared with control *Rrm2b* competent animals (Cr 0.4, BUN 26.0, albumin 3.0, cholesterol 124, triglycerides 93). The kidney tissue from the *Rrm2b* deficient animals demonstrated collapse and retraction of the glomerular capillary tufts with severe mesangiolysis. There was marked visceral and parietal epithelial hypertrophy and vacuolization. Focal segmental lesions, crescents and endocapillary proliferation were not present. There was marked tubular distention with abundant proteinaceous fluid. The epithelial cells lacked distinct brush borders. Electron microscopy revealed diffuse foot process effacement and absence. Microvillous transformation was seen

in some areas. The visceral epithelial cells were markedly vacuolated. The glomerular membranes were of normal thickness, but were folded and wrinkled. There was no basement membrane reduplication. The capillary luminal diameters were severely decreased by hypertrophic endothelial cells. There was a paucity of mesangial matrix and cells.

Conclusions: Ribonucleotide reductase p53R2 deficiency in the p53 DNA repair pathway induces severe glomerular and tubular injury early in life, leading to renal failure with nephrotic syndrome. The mechanism for glomerular disease is most likely related to activation of p53-mediated apoptotic pathways in the absence of p53R2 and lack of deoxyribonucleotides necessary for DNA repair and synthesis.

1571 Benign and Malignant Oncocytic Neoplasms of the Adrenal Cortex Have Different Mitochondrial Morphology: An Ultrastructural and Immunohistochemical Study of 7 Cases

MD Legmann, JR Shia, RA Erlanson, LH Tang, DS Klimstra. Memorial Sloan Kettering Cancer Center, NY.

Background: Cytoplasmic eosinophilia is a common phenomenon in adrenal cortical neoplasms (ACN), mostly due to rich smooth and rough endoplasmic reticulum (SER & RER). True oncocytic features corresponding to abundant cytoplasmic mitochondria are rare. As such, oncocytic ACN have not been fully characterized and little is known about the mechanisms involved in the genesis of neoplastic oncocytes.

Design: We identified 7 oncocytic tumors of the adrenal cortex from the EM files of the department of pathology at Memorial Sloan-Kettering Cancer Center between 1971 and Sept. 2002. All 7 cases were proven by EM to contain abundant cytoplasmic mitochondria. There were 3 adenomas and 4 carcinomas. Histologic, immunohistochemical (IHC) and ultrastructural assessments were performed on all 7 cases. Clinical characteristics were obtained.

Results: While abundant cytoplasmic mitochondria was present in all 7 cases, the mitochondria in adenoma were more uniform with rich and mildly altered cristae, without intramitochondrial granules or densities. In carcinoma, there was apparent mitochondrial hydropia with reduced numbers of cristae, more apparent tubulovesicular pattern, often prominent intramitochondrial granules and flocculent densities. Other fine structural differences included more apparent SER, more stacked RER and more lysosomal granules in adenoma. Histologically, marked cytoplasmic eosinophilia with a granular quality was a common feature in all 7 cases, but carcinoma cases tended to have more variation in cell size and shape with more irregular nuclei. IHC studies on all of the cases displayed the typical phenotype of ACN. Additionally, 2 of the 4 carcinomas stained positively for cytokeratins (AE1:AE3 & CAM 5.2). All adenomas occurred in females, age 27-60 yrs, whereas carcinoma was more common in males (3:1), with a narrower age range (50-60 yrs). All patients were treated with surgical excision. The 3 adenoma patients were all alive at a follow-up of 31, 119 and 179 mos. Two carcinoma patients died of disease at 1 mo and 34 mos, and 2 were alive at a follow-up of 44 and 56 mos.

Conclusions: We report 7 cases of an unusual type of neoplasm. These findings reinforce the need for EM to establish the diagnosis of oncocytic ACN. Our finding of different ultrastructural morphology of mitochondria between oncocytic adenoma and carcinoma of the adrenal cortex suggests that different mechanisms may be involved in oncocytosis in benign and malignant conditions.

1572 Propensity of Glomerular Endothelial Cell Nuclei to the Mesangial Zone of Capillary Lumina: A New Method for Estimating Linear Interaction of Surfaces

B Najafian, JT Crosson, M Mauer. University of Minnesota, Minneapolis, MN.

Background: Structural properties of tissues can be evaluated by stereology. Interaction of surfaces (how much of one surface is facing another) is related to their relative positions. We provide an unbiased method to estimate linear surface interaction (LSI) of objects, followed by an example that investigates early changes in type 1 diabetic (T1D) patients. Consider the reference space X contains two objects Y_1 and Y_2 , providing $Y_1 \cap Y_2 = \emptyset$. If a test line T isotropically, uniformly and randomly (IUR) sweeps X , it is proved that LSI is related to $\Pr\{T \uparrow Y_1 | T \uparrow Y_2, T \subset X\} / \Pr\{T \uparrow Y_1 | T \subset X\}$, notations: \Pr =probability; \uparrow =intersection; $\hat{=}$ estimate; $E\{\}$ =mean; I = # intersections. Then $LSI = E\{I(T \uparrow Y_1 | T \uparrow Y_2) / E\{I(T \uparrow Y_1)\}$, if T is IUR in X and profiles of Y_1 and Y_2 are entirely visible on planes of estimation.

Design: Renal biopsies from 5 kidney donors (C), age 30 ± 8 (mean \pm SD) years and 5 normoalbuminuric (NA) T1D patients, age 29 ± 5 and T1D duration 15 ± 5 years were studied by electron microscopy (EM). Random profiles of 1-3 glomeruli (G)/biopsy were prepared. EM images at $4,800\times$ were obtained to make montage images of G profiles. Capillary lumen walls were divided into peripheral (PL) and mesangial (ML) zones at the anchor points. A lattice grid was superimposed on images. Intersections of lines with basal surface of endothelial nuclei (BSEN), PL and ML were counted. LSI of BSEN with ML (LSI_m) was estimated.

Results: LSI_m was $53.6 \pm 11.7\%$ in C and $50.5 \pm 12.0\%$ in NA [p =nonsignificant (NS)]. Fraction of lumina which is ML [$S_s(ML/L)$] was $29.6 \pm 0.9\%$ in C and $27.0 \pm 11.8\%$ in NA (p =NS). Since estimations were done in IUR condition, if endothelial nuclei are randomly located along the lumina, it is theoretically expected, that LSI_m approaches $S_s(ML/L)$. The estimated LSI_m was different from $S_s(ML/L)$ ($p < 0.02$ and $p < 0.002$ for C and NA). The difference of LSI_m from $S_s(ML/L)$, Δ , is deviation from randomness. Δ was $24.0 \pm 12.5\%$ (C) and $18.1 \pm 5.4\%$ (NA), p =NS. The ratio of BSEN to total lumen surface was not different in C (0.12 ± 0.05) and NA (0.12 ± 0.03).

Conclusions: A new method is described for estimating LSI. The results show that there is a tendency for endothelial nuclei to be on mesangial zone of glomerular capillary lumina in C and NA with no difference between the two groups. This propensity may provide more fenestrated cytoplasm on PL. Further studies are required to uncover the basis for this phenomenon and possible changes in this tendency in pathological conditions.

1573 Ultrastructural Heterogeneity in Post Infectious Glomerulonephritis

TN Pham, TA Fields, DN Howell. Duke University Medical Center, Durham, NC; Durham VA Medical Center, Durham, NC.

Background: Post-infectious glomerulonephritis (PIGN) is a frequent cause of acute renal failure. PIGN most often affects children and young adults and usually resolves with supportive therapy. While the majority of patients with PIGN do not undergo renal biopsy, microscopic evaluation remains an important tool for distinguishing PIGN from renal diseases that may require specific therapy. Renal biopsies of PIGN typically show diffuse proliferative glomerulonephritis (DPGN) with neutrophils and glomerular deposits of C3 and IgG. However, the most consistent diagnostic change is generally reported to be large subepithelial deposits ("humps") seen by electron microscopy (EM). We report a series of 12 cases of PIGN with a variety of EM findings, including most in which the predominant pattern of deposits is not subepithelial "humps."

Design: From the Duke University database, we identified 12 cases with clinical and/or pathologic features PIGN from 2/96 to 9/04. All cases were evaluated by light microscopy and EM. Immunofluorescence (IF) microscopy was performed in 11 of 12 cases. Clinical records of the patients were reviewed to assess both pre-biopsy history and post-biopsy course.

Results: Eleven patients had clinical evidence of infection: 4 with a positive culture (all *Staphylococcus aureus*), 3 with increased anti-Streptolysin O titers, and 4 with other signs/symptoms of infection. The other patient's biopsy had typical features of PIGN, including prominent subepithelial humps. Most cases exhibited DPGN (10/12); the other cases showed mesangial proliferative glomerulonephritis. Most showed extensive neutrophil exudation (9/12). IF revealed dominant or co-dominant C3 staining in all cases. EM revealed subepithelial deposits in most cases (9/12), although 6 showed predominantly subendothelial deposits, and 3 showed mostly mesangial. Two cases demonstrated a predominance of subepithelial "humps," and one was a mix of intramembranous and subepithelial deposits. Follow-up was available for 9 patients. Seven patients had improved renal function with only supportive therapy and/or low dose steroids. One patient had spontaneous improvement in serum C3 levels but continued proteinuria, and 1 patient developed chronic renal insufficiency.

Conclusions: Renal biopsies from patients with typical clinical and light microscopic and IF features of PIGN may demonstrate a variety of ultrastructural findings, including predominant subendothelial and mesangial deposits.

1574 In Situ Visualization of Ferritin and Hemosiderin in Alzheimer's Disease Hippocampus by Tem and X-Ray Nanoanalysis

C Quintana, S Bellefqih, JY Laval, A Gloter, A Croisy. Institut Curie, Paris, France; GHU Pitie-Salpetriere, Paris, France; Laboratoire de Physique du Solide, Paris, France.

Background: Excess brain iron is a consistent observation in neurodegenerative disorders, notably in Alzheimer's disease (AD). The ferritin (Ft), the main protein involved in iron storage, was detected in paired helical filaments isolated from AD. Fifty percent of this Ft has a chemical composition different from horse spleen Ft and human liver Ft, corresponding to the composition of iron hemosiderin (Hm).

Design: The aim of this study is to verify the presence of Ft and Hm in subcellular localization in hippocampal samples from patients with AD (n=3) and from non demented control patients (n=3). Ft and Hm have been identified in unstained and lightly stained thin sections. We confirm the presence of iron in both types of molecules by using X-Ray nanoanalysis.

Results: Ultrastructural examination showed ferritin molecules in the nucleus and in the cytoplasm of glial cells. It was observed in and around senile plaques (SP) and bound to neurofibrillary tangles. It was always associated with pseudo-myelinic structures within dystrophic neurites. Hemosiderin was found in reactive glial cells surrounding SP.

Conclusions: Iron associated to Hm is readily released and may cause cell damage. The presence of Hm in hippocampus of AD patients seems to confirm the hypothesis that Hm is related to a dysfunction of Ft, associated with an increase level of brain ferrous toxic iron, that may contribute to the production of free hydroxyl radicals and thus, to neuronal death.

1575 The Importance of Ultrastructural Evaluation of Tubular Casts in Renal Biopsies in Adults

NO Uribe-Urbe, GA Herrera. LSU Health Sciences Center, Shreveport, LA.

Background: Tubular casts are often found in a variety of conditions. Ultrastructural evaluation of casts has not been critically and systematically performed to define its usefulness from a pathological and clinical perspective.

Design: Fifty three consecutive renal biopsies, routinely processed for light microscopy (LM), immunofluorescence (IF), and electron microscopy in which casts were identified in thick sections prepared for ultrastructural survey, were subjected to blind, critical, ultrastructural evaluation. The patients' average age was 58.4 years (17-88); there were 27 males and 26 females, with a wide variety of renal diseases.

Results: As expected, the great majority of the casts were in the distal nephron. The majority of the casts (43.4%) were homogeneously eosinophilic in appearance (hyaline) by LM and shared IF staining for both light chains IgM and IgA. Ultrastructurally, these casts were generally composed of homogeneous electron dense material. One third (33.9%) of the cases showed admixed hyaline casts and casts composed by cellular debris with granular material (CDG); only five cases (9.4%) had exclusively CDG casts. These three types of casts were associated with a wide variety of diseases (focal and segmental glomerulosclerosis, diabetes mellitus glomerulosclerosis, vascular sclerosis, membranoproliferative glomerulonephritis (GN), membranous GN, etc.). In 13% of the cases, the morphology of the casts was distinctive enough to indicate specific compositions. Three cases with red blood cell cast (5.6%) were associated with necrotizing glomerulopathy, and IgA nephropathy. Two cases with crystalized

light chain casts (3.7%), one kappa and one lambda highlighted by corresponding 3+ IF staining, were associated with plasma cell dyscrasias. One case of acute pyelonephritis with polymorphonuclear cell casts, and one case with myoglobin casts, noted after strenuous exercise, and cocaine abuse were also identified.

Conclusions: Ultrastructural evaluation of casts may provide useful information that, in some cases, may be critical to establish or suggest a specific diagnosis.

1576 DC-LAMP Is a Specific Marker for Human Bronchiolar Clara Cells

L Zhu, AL Moreira, J Yim, ND Cassai, GS Sidhu. New York University School of Medicine, New York, NY.

Background: Alveolar type II pneumocytes (PII) and bronchiolar Clara cells (CC) stain with mAb PE-10 (surfactant apoprotein). Adenocarcinoma of CC type cannot be easily distinguished from those of PII type. DC-LAMP (lysosomal associated membrane protein) is a molecule expressed in dendritic cells, but its mRNA is also expressed in lung. This study compares the immunostaining spectrum of PE-10 and DC-LAMP in normal and neoplastic lung using EM to define cell type.

Design: Sections of normal lung (5), and lung adenocarcinoma (47) were stained with PE-10 and DC-LAMP. Of the 47, 14 were bronchioloalveolar carcinomas (BAC), 12 invasive, and 21 mixed. Two more cases of BAC, known by EM to be pure CC type and pure TII type respectively were examined by PE-10 and DC-LAMP staining. EM was done on 6 BAC from the group of 47 to define cell type.

Results: PE-10 stains alveolar and bronchiolar epithelium, but DC-LAMP stains mainly alveolar macrophages and Clara cells (distal respiratory bronchiolar epithelium). The latter stain weakly with PE-10. An EM-proven Clara cell BAC (Fig 1B) was DC-LAMP strongly positive (Fig 1A), but PE-10 weakly positive, and an EM-proven type II pneumocyte (Fig. 1D) was PE-10 positive and DC-LAMP negative(1C). DC-LAMP staining of the 47 lung adenocarcinomas showed positivity in 21.4% (3/14) of BAC group, 28.6% (6/21) of mixed-subtype and 25% (3/12) of invasive adenocarcinomas, indicating persistent Clara cell differentiation. EM on 6 of the 14 BAC showed Clara cell type in 3 with strong DC-LAMP and weak PE-10 staining, and type II pneumocyte type in 3 with negative DC-LAMP and positive PE-10 staining.

Conclusions: DC-LAMP specifically stains human Clara cells without cross-reactivity with type II pneumocytes. Thus, it can be used for identifying primary or metastatic Clara cell type adenocarcinomas of lung. It could also be used to target Clara cells in mAb-dependent imaging and therapy. We are currently examining use of DC-LAMP in a diagnostic panel to augment the value of TTF-1 and PE-10 mAb in FNA biopsy specimens of primary and metastatic pulmonary tumors.

